RSC Advances

PAPER

View Article Online
View Journal | View Issue

Cite this: *RSC Adv.*, 2021, **11**, 10243

Ru-containing magnetic yolk–shell structured nanocomposite: a powerful, recoverable and highly durable nanocatalyst

Reza Mirbagheri,[a] Dawood Elhamifar *[a] and Shaaker Hajati[ab]

Received 7th December 2020
Accepted 1st February 2021

DOI: 10.1039/d0ra10304g

rsc.li/rsc-advances

A novel method was used to prepare a magnetic phenylene-based periodic mesoporous organosilica nanocomposite with yolk–shell structure (Fe_3O_4@YSPMO). The Fe_3O_4@YSPMO nanomaterial was prepared by using easily accessible pluronic-P123 and cetyltrimethylammonium bromide (CTAB) surfactants under basic conditions. This material was employed for effective immobilization of potassium perruthenate to prepare an Fe_3O_4@YSPMO@Ru nanocatalyst for the aerobic oxidation of alcohols. The physiochemical properties of the designed Fe_3O_4@YSPMO@Ru nanocomposite were studied using PXRD, FT-IR, TGA, SEM, TEM, ICP, VSM and XPS analyses. Fe_3O_4@YSPMO@Ru was effectively employed as a highly recoverable nanocatalyst in the selective aerobic oxidation of alcohols.

1. Introduction

On the topic of supported heterogeneous catalysts, the structure and morphology of supports are important properties that can affect the catalyst performance. For example, the surface area of a permeable hallow sphere-supported catalyst is much more than a core–shell one because of its accessible inner layer. Yolk–shell (YS) nanocomposites are known as a new member of the hollow nanoarchitecture family with advantages of high surface area, tunable physiochemical properties, high capacity for adsorption and/or catalyst immobilization and high stability.[1–3] The easy functionalization of both cores and shells made the YSs an attractive candidate for different applications such as drug delivery and nanocatalysis.[4–9] Especially, YS-structured nanomaterials with mesoporous silica shells are very interesting to chemists owing to their attractive properties such as high stability, non-toxicity, high stability, biocompatibility and biodegradability as well as high surface area and pore volume.[10,11] On the other hand, among different cores, the Fe_3O_4 NPs are more interested in the synthesis of YS-structured materials due to the advantages of low-cost, high magnetic properties, high loading of OH on their surface and also easy preparation.[12,13]

Different methods have been used for the preparation of YS nanocomposites that can be divided into template-assisted and template-free approaches. The well-known template-less methods are Kirkendall[14,15] and Ostwald ripening.[16–19] Based on the type of surfactant, template-assisted methods are divided into hard[20] and soft[21] approaches. In the hard approach, the template is located between the core and shell. This template is selectively removed under special conditions to prepare the YS-structure. The disadvantage of tedious processing steps, makes the hard-template method inefficient. The soft-template assisted method has recently been employed as a simple and efficient strategy to prepare YS nanocomposites. To date, a few unusual and/or less-available surfactants have been used as a soft template to prepare YS materials.[22–25] Some recently developed surfactants applied in this matter are SDBS and LSB,[18] water/oil (W/O) microemulsions such as Igepal CO-520 (NP-5) and cyclohexane in water,[26] FC4 with pluronic F-127 (ref. 24) and also FC4 with cetyltrimethylammonium bromide (CTAB).[25]

As mentioned above, most of these surfactants are expensive and commercially unavailable. Therefore, the preparation of novel yolk–shell nanocomposites using routine, low-cost and easily available soft-templates is a very important progress in this matter.

On the other hand, oxidation is a very important process in chemistry, due to its diverse industrial applications such as ground remediation with trichloroethylene (TCE) or tetrachloroethylene (PCE),[27,28] pesticides removal,[29] formaldehyde removal[30–33] and elimination of chemical oxygen demand (COD) for industrial waste water,[34] *etc.* Especially, the oxidation of alcohols to respective carbonyls is an important subject in organic synthesis. Various reagents and catalysts such as chromium oxide,[35–39] manganese oxide,[40–42] activated DMSO,[43–46] hypervalent iodine,[47–49] pyridine-SO_3 (ref. 50) and NaOCl with TEMPO[51–55] have been used for the oxidation of alcohols. Among different oxidants, molecular oxygen is of more interest due to its availability, low-cost and especially the production of water

[a]*Department of Chemistry, Yasouj University, Yasouj 75918-74831, Iran. E-mail: d.elhamifar@yu.ac.ir; dawood.elhamifar@gmail.com; Fax: +98-74-33223048; Tel: +98-74-33223048*

[b]*Department of Semiconductors, Materials and Energy Research Center (MERC), P.O. Box 31787-316, Tehran, Iran*

as only by-product. However, these homogeneous systems suffer from restrictions such as difficulty in catalyst and product separation and waste problems. Therefore, the use of heterogeneous catalysts has been highly developed in this matter. Some of recently developed catalytic systems are based on noble metals such as Pd[56–64] and Ru.[65–71] A number of reported studies in this matter are hydroxyapatite-supported palladium nanoclusters,[72] methyl glycolate-supported gold,[73] carbon-supported Pt, Pt–Ru and Pt_3Sn,[74] graphene-supported Pt and Pt–Ru,[75] silica-supported TEMPO,[76] PMO-IL@RuO_4 (ref. 77) and ILNOS-Ti.[78]

In view of the above, herein, a novel soft-template assisted strategy has been developed for easy preparation of magnetic phenylene-based ordered mesoporous nanocomposite with yolk–shell structure (Fe_3O_4@YSPMO). Pleasingly, for the first time, the routine, easily available and low-cost surfactants (pluronic P123 and CTAB) were used as a template to prepare the Fe_3O_4@YSPMO nanomaterial (Scheme 1).

2. Experimental section

2.1 Preparation of Fe_3O_4@YSPMO nanocomposite

Magnetic Fe_3O_4 nanoparticles were synthesized according to our recently reported procedure.[79] In order to prepare Fe_3O_4@YSPMO, the Fe_3O_4 NP (0.12 g) was first completely dispersed in distilled water (25 mL) and then this was added to

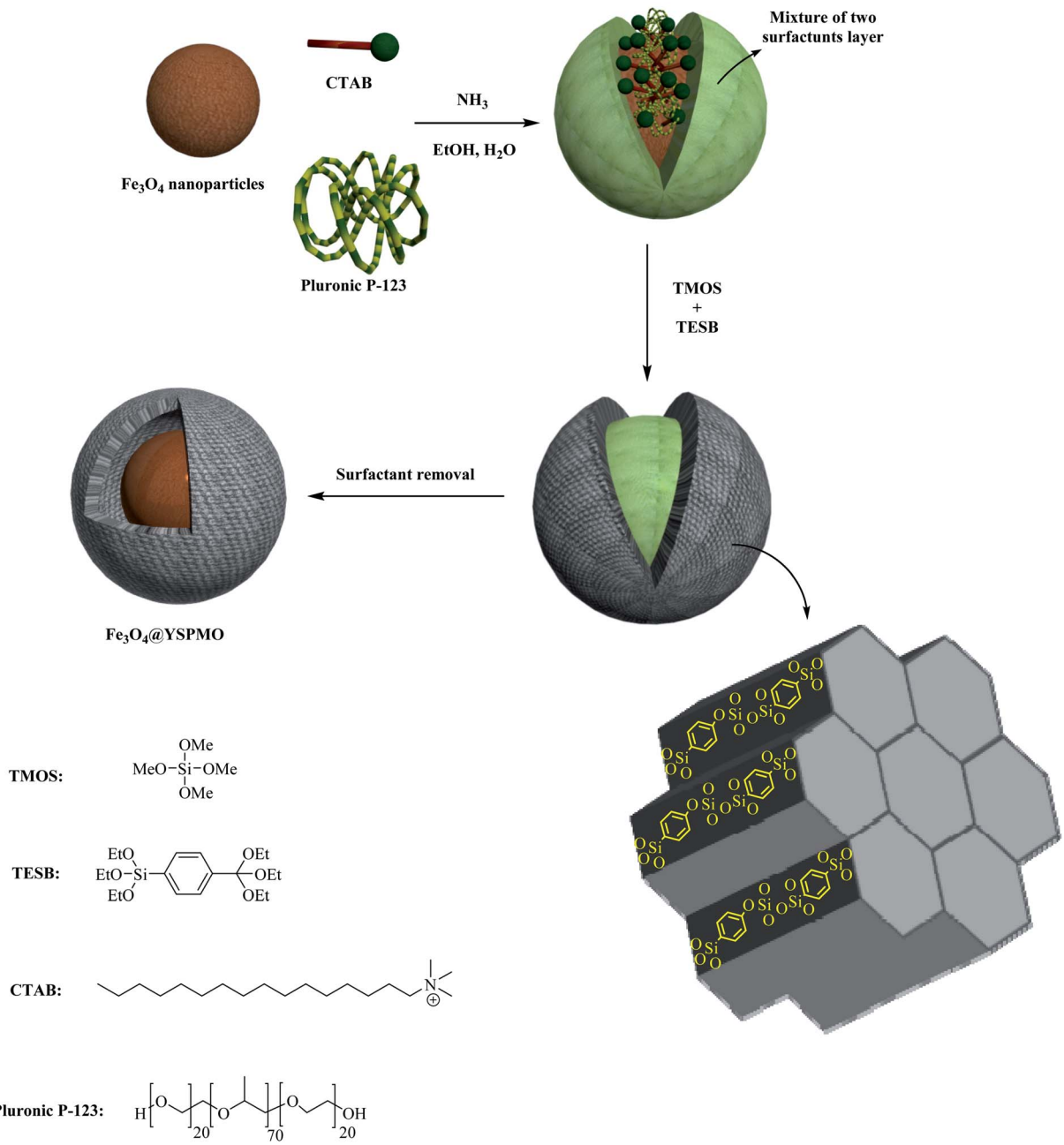

Scheme 1 Preparation of Fe_3O_4@YSPMO nanocomposite.

a solution of ethanol (16 mL) and water (36 mL) containing CTAB (0.32 g), pluronic P123 (0.52 g) and ammonia (0.4 mL). The resulted mixture was stirred at 35–40 °C. After 30 minutes, TMOS (0.31 mL) and TESB (0.85 mL) were added and the stirring was continued for 1 hour. Next, the obtained combination was heated at 100 °C statically for 17 hours. The final material was collected and washed with H_2O and EtOH. The pluronic P123 and CTAB surfactants were removed using a Soxhlet apparatus using acidic ethanol (Scheme 1).

2.2 Preparation of Fe_3O_4@YSPMO@Ru

Firstly, 0.4 g of Fe_3O_4@YSPMO nanoparticles were dispersed in water (15 mL) under ultrasonic irradiations. Then, potassium perruthenate (0.05 g) was added and the mixture was stirred at RT for 12 h. The resulted material was collected and washed several times with water and acetone to remove unsupported potassium perruthenate. Finally, the product was dried at 50 °C for 8 h and it was denoted as Fe_3O_4@YSPMO@Ru (Scheme 2).

2.3 Procedure for the oxidation of alcohols using Fe_3O_4@YSPMO@Ru

Typically, alcohol (1 mmol) and catalyst (0.3 mol%) were added in a reaction vessel containing TFT (10 mL) and it was stirred at 90 °C under O_2 gas (1 atm). The progress of reaction was monitored by GC. After the oxidation process was completed, the catalyst was easily removed using an external magnetic field. The yield and conversion were calculated *via* GC results.

3. Results and discussion

For the preparation of Fe_3O_4@YSPMO@Ru nanocomposite, firstly, magnetic iron oxide NPs were prepared.[80] The Fe_3O_4 nanoparticles were then modified with periodic mesoporous organosilica shell as follows. The Fe_3O_4 NPs were completely dispersed in an aqueous ethanol solution containing ammonia,

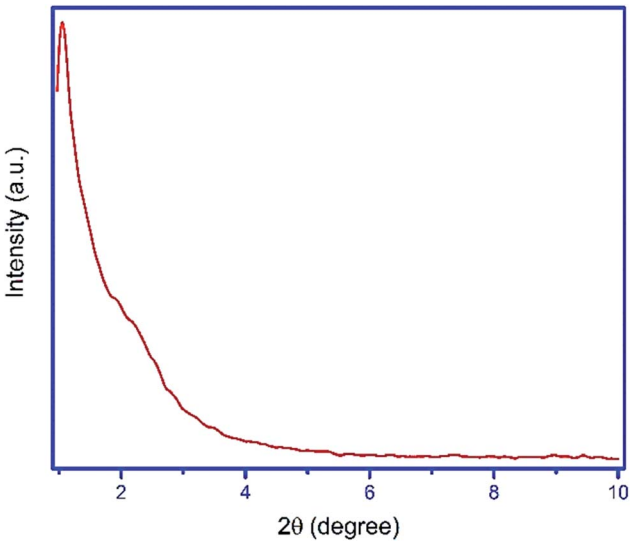

Fig. 1 The low-angle powder XRD pattern of Fe_3O_4@YSPMO@Ru.

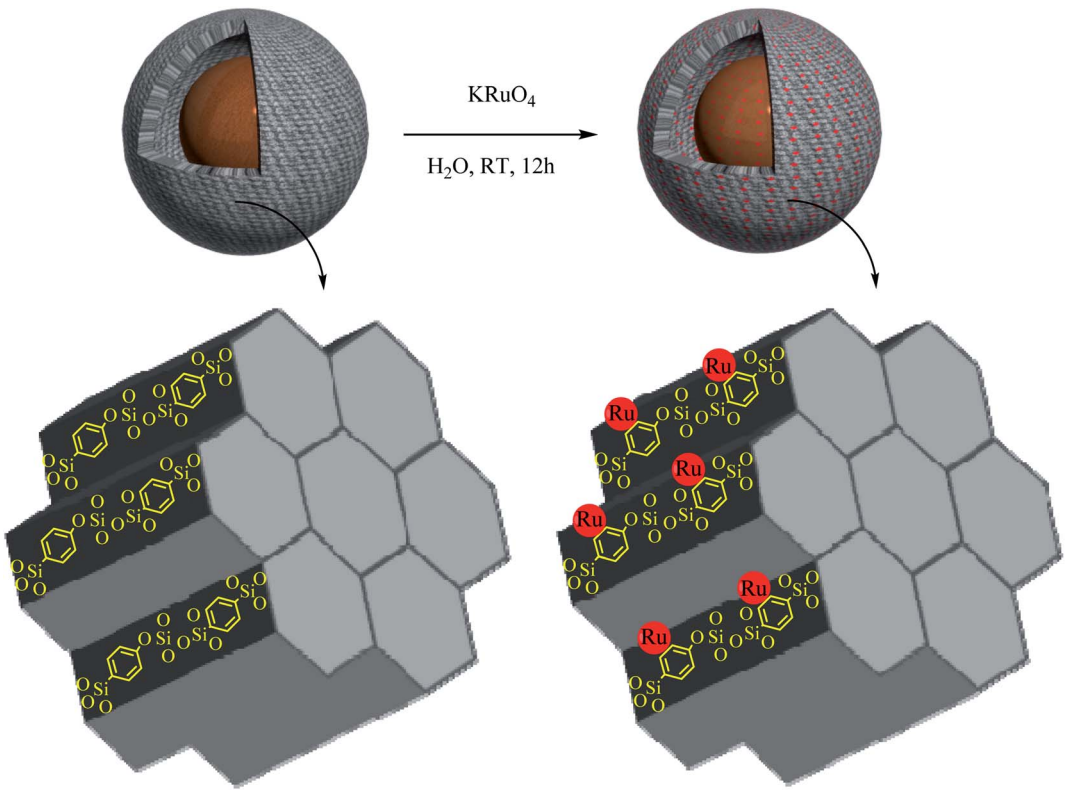

Scheme 2 Preparation of Fe_3O_4@YSPMO@Ru nanocomposite.

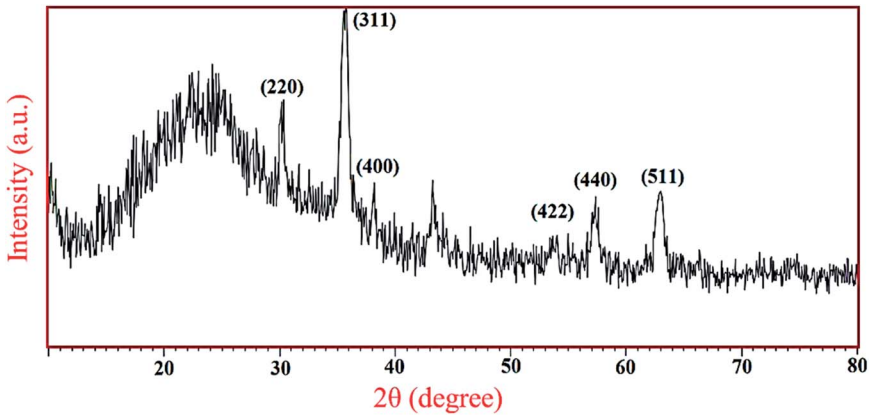

Fig. 2 The wide-angle PXRD pattern of Fe_3O_4@YSPMO@Ru.

CTAB and P123. After 30 minutes stirring, the TMOS and TESB precursors were added as the source of silica. This mixture was stirred for 1 h at 35–40 °C. The obtained mixture was then statically heated at 100 °C to form mesoporous organosilica shell. Importantly, in this study, for the first time, the routine and easily available surfactants (CTAB and pluronic P123) were used as structure-directing agents under moderate conditions to prepare yolk–shell structured Fe_3O_4@YSPMO material (Scheme 1). The Fe_3O_4@YSPMO was used for the immobilization of potassium perruthenate to prepare a powerful nanocatalyst named Fe_3O_4@YSPMO@Ru (Scheme 2). This nanomaterial was characterized using different techniques and applied as highly recoverable catalyst in the aerobic oxidation of alcohols.

The low-angle powder XRD pattern (Fig. 1) demonstrated a sharp d_{100} peak at 2θ of about 1° confirming the presence of periodicity in a shell with two-dimensional hexagonal structure for the catalyst. According to this peak, it can be concluded that none of the surfactants lonely exists in the outer layer and the final form of the shell is made through a combination of both surfactants.

Furthermore, the wide-angle PXRD was in agreement with Fe_3O_4 spinel structure and showed six peaks at 2θs of 30, 35, 43, 54, 57 and 64° corresponding, respectively, to the *Miller indices* (*hkl*) values of 220, 311, 400, 422, 440 and 511. The broad peak appeared at 2θ over 20–27 degree is also related to mesoporous silica shell (Fig. 2).

The FT-IR spectra of Fe_3O_4 NPs and also Fe_3O_4@YSPMO before and after the extraction of surfactants are shown in Fig. 3. These showed a peak at 573 cm^{-1} corresponding to Fe–O bond for all materials. The O–H bonds of material surface were appeared about 3400 cm^{-1}. Interestingly, new bands were observed for Fe_3O_4@YSPMO, before and after the surfactant extraction (Fig. 3(B) and (C)). Before the surfactant extraction,

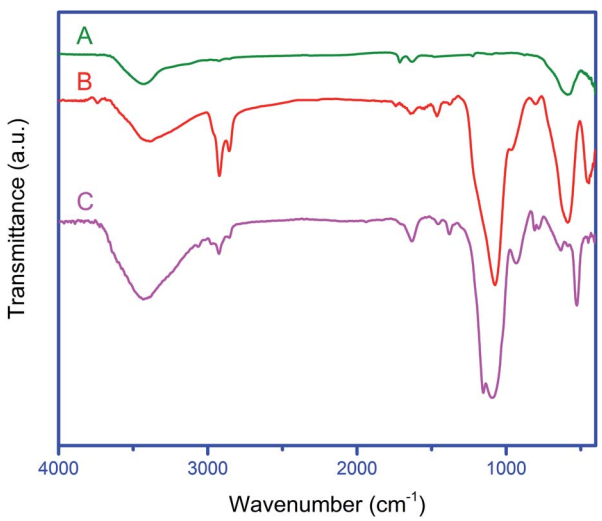

Fig. 3 The FT-IR spectra of Fe_3O_4 (A), Fe_3O_4@YSPMO nanoparticles before (B), and after (C) surfactant extraction.

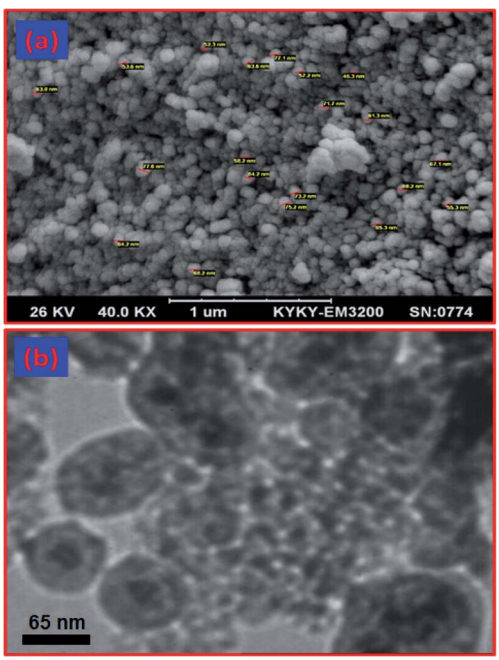

Fig. 4 SEM (a) and TEM (b) images of the Fe_3O_4@YSPMO@Ru nanomaterial.

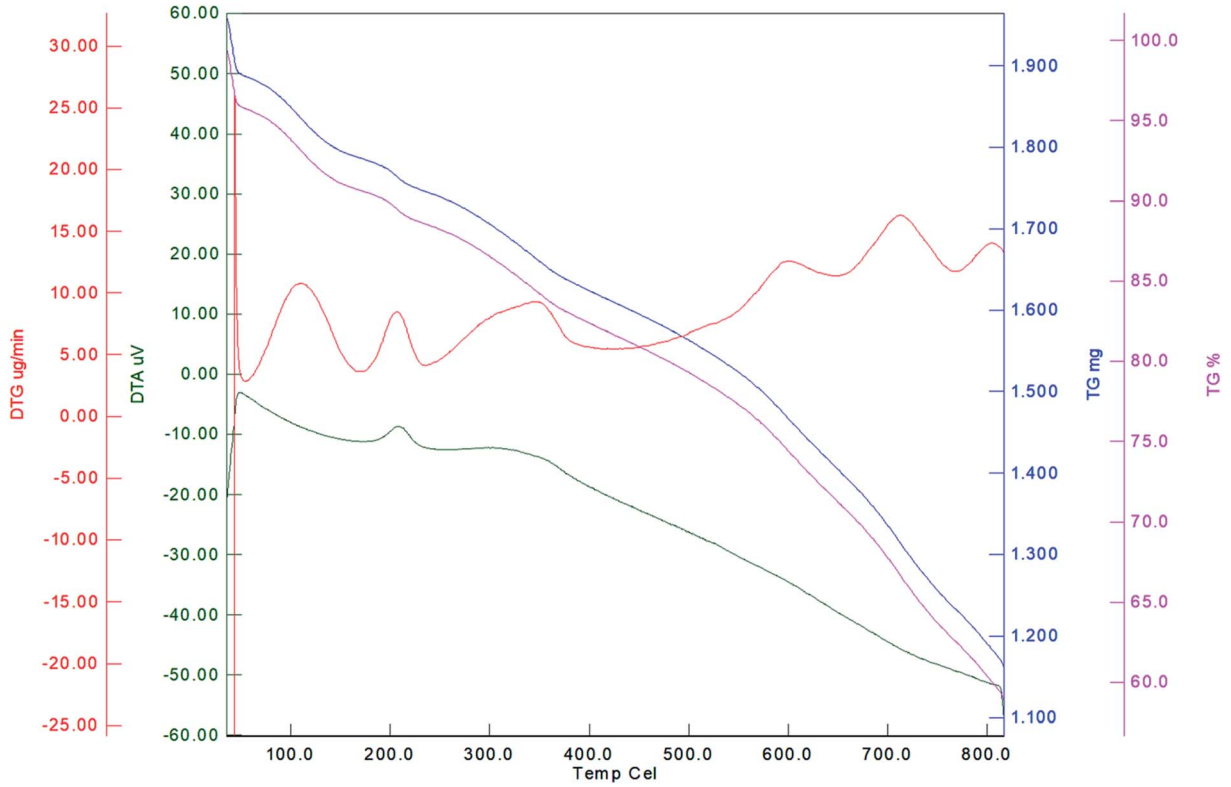

Fig. 5 TGA pattern of Fe_3O_4@YSPMO@Ru.

the bands observed at 2922 and 2853 cm^{-1} are due to the aliphatic C–H bonds of P123 and CTAB surfactants (Fig. 3(B)). After the Soxhelet extraction, the latter signals were not seen confirming well removal of surfactants during extraction process (Fig. 3(C)). The peaks at 720–810 cm^{-1} are attributed to C–Si bonds. Moreover, the bands at 1096 and 932 cm^{-1} are due to symmetric and asymmetric vibrations of Si–O–Si bonds. The bands appeared around 3100 cm^{-1} are corresponded to aromatic C–H bonds of PMO shell. The C=C bonds of phenylene rings were also observed at 1630 cm^{-1}. These results

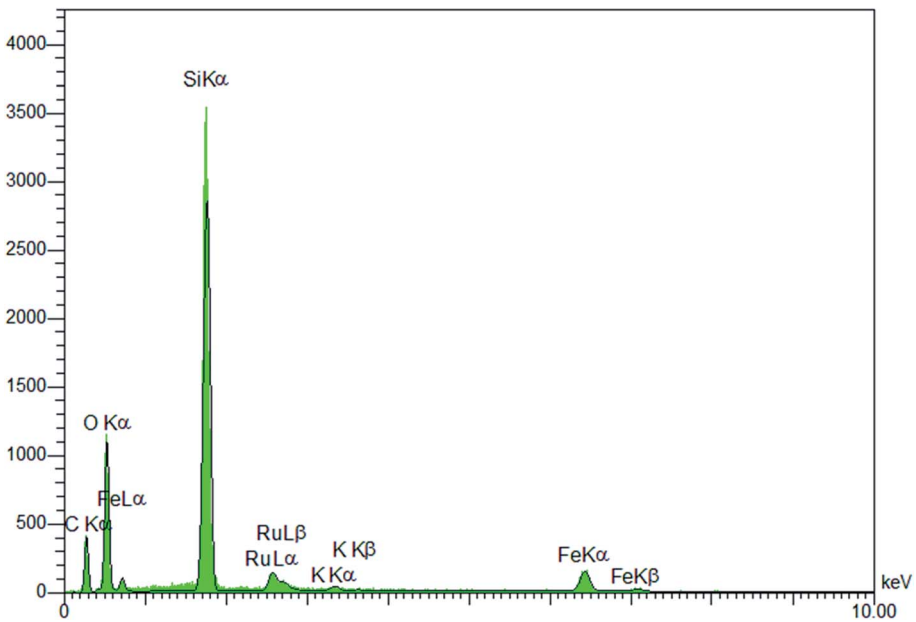

Fig. 6 EDS spectrum of Fe_3O_4@YSPMO@Ru.

confirm successful formation of phenylene-PMO-shell around magnetite NPs.

Scanning electron microscopy (SEM) image is shown in Fig. 4(a). This image showed uniform spherical particles with an average size of 70 nm for the material. The transmission electron microscopy (TEM) image of Fe_3O_4@YSPMO is shown in Fig. 4(b). This also showed YS-structured spherical particles with a void space between black cores (Fe_3O_4 NPs) and gray shells (organosilicas) for the designed material.

Thermal stability of Fe_3O_4@YSPMO@Ru was studied by TGA (Fig. 5). A weight loss of about 6% below 120 °C is attributed to elimination of remained H_2O, EtOH and MeOH from the synthetic process. The second weight loss (about 7%) was found at 121–300 °C corresponding to remained surfactants during extraction process. The main weight loss (27%) at 301–800 °C is due to removal of the phenylene moieties incorporated into material shell.

Immobilization of potassium perruthenate in the prepared material was investigated by using EDS and ICP analyses. The EDS pattern (Fig. 6) proved the presence of Ru, O, Si, Fe and C in the material. The exact amount of ruthenium was calculated by ICP (2.38 mol%). These data were found to be in good agreement with FT-IR and TGA results confirming well incorporation/immobilization of phenylene and perruthenate moieties into/onto material framework.

The VSM analysis was also performed to investigate the magnetic properties of the designed catalyst (Fig. 7). According to this, the saturation magnetization of Fe_3O_4@YSPMO@Ru nanocomposite was found to be about 14 emu g^{-1} confirming good magnetic properties of the catalyst.

The XPS survey spectrum (Fig. 8) of the nanocomposite was taken and analyzed to investigate its chemical composition. Before the XPS analysis, Savitzky–Golay filtering was implemented on the XPS spectra to reduce their noise level.[81,82] All signals were calibrated to have C 1s at BE of 284.9 eV. As shown in Fig. 8, Si $2p_{3/2}$ is observed at 103.27 eV, which confirms its contribution in the PMO part of the material as SiO_2. The peak of Ru $3p_{3/2}$ appeared at binding energy of 463.5 eV confirming the presence of Ru as Ru (4+). It was also found that the oxygen contributes in the material as SiO_2 (533 eV) and RuO_2 (530.2 eV). Iron and potassium were not found in XPS spectra though they were shown to be present in the material by using EDS. As known, EDS is a characterization technique for analyzing bulk materials and thus it was able to detect Fe from Fe_3O_4 as core material. Despite EDS, XPS is a surface sensitive technique with sampling depth of three times of inelastic scattering mean free path of electrons (IMFP) with a given kinetic energy within a given overlayer. For instance, the IMFPs of Fe 2p electrons with kinetic energy of about 543 eV within the overlayers of SiO_2 and RuO_2 are calculated from Tanuma–Powell–Penn (TPP) formula to be 1.85 and 1.11 nm, respectively. In other words, the escape depth of such electrons within SiO_2 and RuO_2 are about 5.55 and 3.33 nm. This indicates that the thickness of the RuO_2/PMO shell enveloping the core Fe_3O_4 is larger than the escape depth of Fe 2p electrons. The relative sensitivity factor for Ru 3p

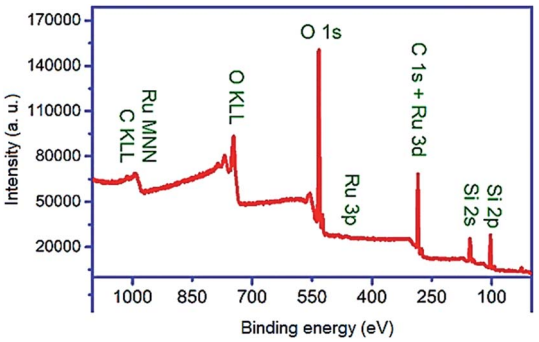

Fig. 8 XPS spectrum of Fe_3O_4@YSPMO@Ru catalyst.

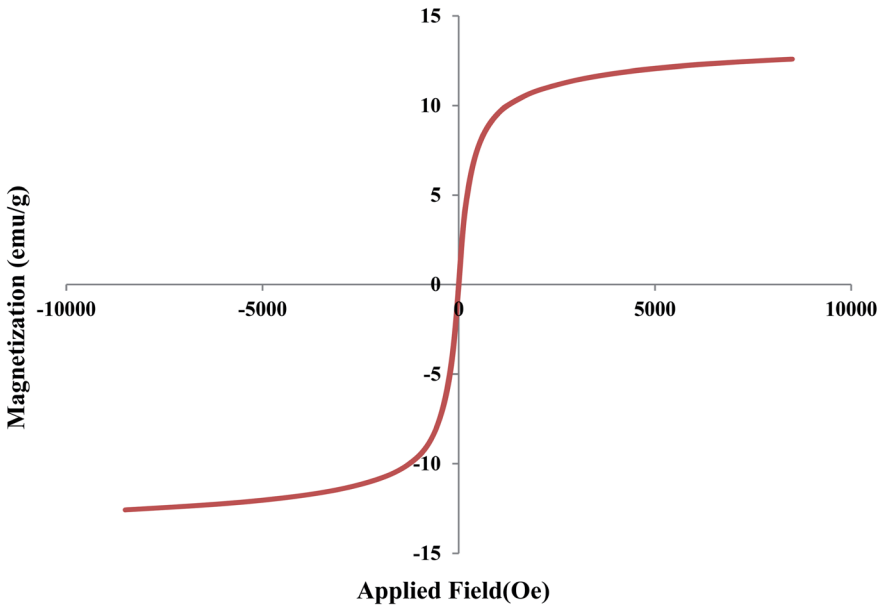

Fig. 7 VSM pattern of Fe_3O_4@YSPMO@Ru.

Table 1 Screening different parameters in 1-phenylethanol oxidation using Fe_3O_4@YSPMO@Ru[a]

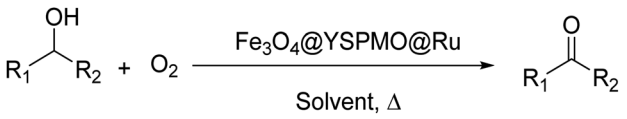

Entry	Catalyst (mol%)	Solvent	Temperature (°C)	Time (h)	Yield[b] (%)
1	0.1	—	R.t.	12	—
2	0.1	Toluene	R.t.	12	10
3	0.1	Toluene	60	12	55
4	0.1	Toluene	90	12	67
5	0.2	Toluene	90	12	80
6	0.2	TFT	90	12	96
7	**0.3**	**TFT**	**90**	**6**	**96**
8	0.3	TFT	75	6	78
9[c]	0.3	TFT	90	6	94
10[d]	0.3	TFT	90	6	68

[a] Conditions: 1-phenylethanol (1 mmol), O_2 (1 atm). [b] GC yield. [c] The Fe_3O_4@YSPMO@Pd was used as catalyst. [d] The Fe_3O_4@YSPMO@Au was used as catalyst.

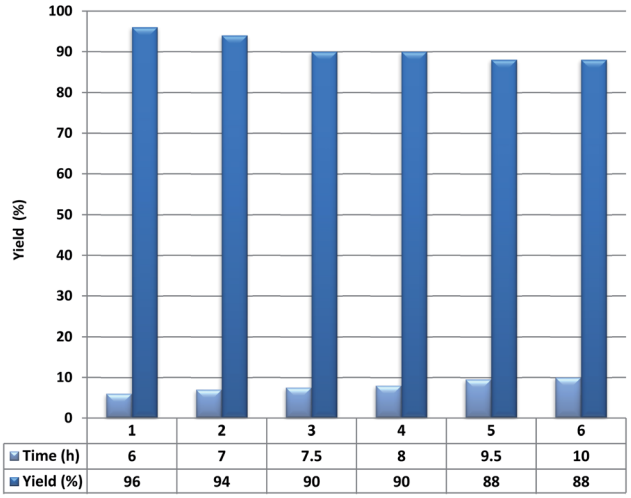

Fig. 9 Recoverability of Fe_3O_4@YSPMO@Ru.

is much higher than that of other elements in the prepared core shell that should result in a Ru 3p signal of high intensity. In spite of this, it is of low intensity, which indicates that to the amount of RuO_2 is very low. Therefore, the disappearance of Fe signal is mainly attributed to the thick PMO layer.

The interaction of aromatic compounds and metal complexes is an important subject because of its importance in the fields of nucleic acids,[83,84] proteins,[85,86] crystal engineering,[87] material science[88] and drug design. Especially in ruthenium–arene complexes, an important interaction is between π-electrons of aromatic rings and the Ru cationic sites with high oxidation states.[89,90] This kind interaction leads to both immobilization and reduction of Ru species. In the present study, we used potassium perruthenate with the oxidation state of +7 for Ru. However, the XPS analysis showed that the oxidation state of supported Ru is +4 in the designed nanocomposite. This is an evidence of successful immobilization of ruthenium species on the organosilica shell that can be achieved *via* coordination of aromatic π-electrons with the Ru-centers followed by the reduction of the oxidation state of Ru from +7 to +4.

After the successful preparation and characterization, the Fe_3O_4@YSPMO@Ru was used as an effective and recoverable catalyst for aerobic oxidation of alcohols. To obtain the best conditions, the oxidation of 1-phenylethanol was selected as a test model. As shown in Table 1, the reaction progress is greatly influenced by the amount of catalyst, solvent and temperature. Accordingly, the best result was obtained using

Table 2 Aerobic oxidation of alcohols catalyzed by Fe_3O_4@YSPMO@Ru[a]

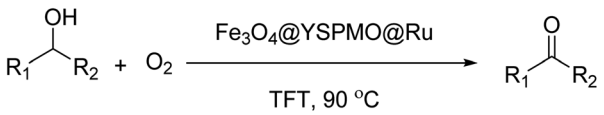

Entry	Alcohol	Time (h)	Yield[b] (%)	TON[c]	TOF[d] (h^{-1})
1	Benzyl alcohol	5	98	326.7	65.3
2	4-Chlorobenzyl alcohol	6.5	94	313.3	48.2
3	4-Methoxybenzyl alcohol	4.5	98	326.7	72.6
4	1-Phenylethanol	6	96	320	53.3
5	1-Phenylpropanol	6	95	316.7	52.8
6	Benzhydrol	12	92	306.7	25.6
7	Cinnamyl alcohol	24	68	226.7	9.4
8[e]	2-Octanol	24	68	136	5.7
9[e]	Cycloheptanol	24	73	146	6.1
10[e]	3-Phenyl-1-propanol	16	56	112	7

[a] Conditions: alcohol (1 mmol), O_2 (1 atm), catalyst (0.3 mol%) in TFT at 90 °C. [b] GC yields. [c] TON: defined as [mmol of product/mmol of catalyst]. [d] TOF: defined as [TON/time]. [e] Conditions: alcohol (1 mmol), O_2 (1 atm), catalyst (0.5 mol%) in TFT at 90 °C.

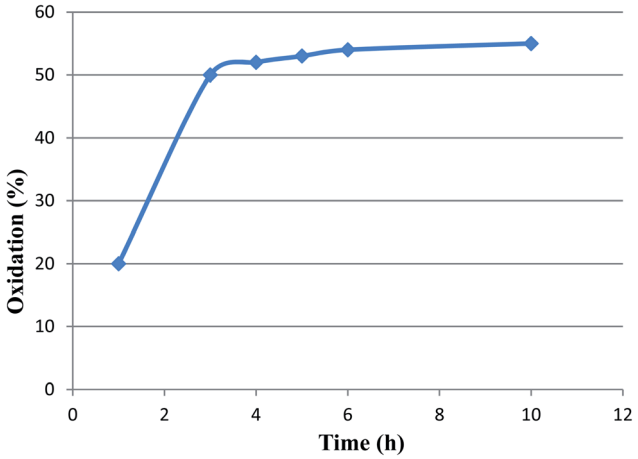

Fig. 10 The effect of hot filtration test in the oxidation process.

0.3 mol% of Fe_3O_4@YSPMO@Ru catalyst in trifluorotoluene (TFT) at 90 °C. In the next study, the catalytic activity of our designed Fe_3O_4@YSPMO@Ru nanocatalysts was compared with Fe_3O_4@YSPMO@Pd and Fe_3O_4@YSPMO@Au nanomaterials (Table 1, entry 7 *versus* entries 9 and 10). The result showed that the best result is delivered in the presence of Fe_3O_4@YSPMO@Ru.

After that, the applicability of this conditions for other alcohols was examined (Table 2). As shown, different alcohols are effectively converted to their corresponding carbonyls (Table 2, entries 1–8). It is noteworthy that this process was very selective for oxidation of primary benzylic alcohols to aldehydes without the formation of appreciable amounts of carboxylic acids (Table 2, entries 1–3). Moreover, 1-phenylpropanol, 1-phenylethanol and benzhydrol also delivered corresponding ketones in high yields (Table 2, entries 4–6). Interestingly, the Fe_3O_4@YSPMO@Ru was also effective in the selective oxidation of cinnamyl alcohol and the corresponding α,β-unsaturated carbonyl was produced in a good yield (Table 2, entry 7). The primary and secondary aliphatic alcohols (both acyclic and cyclic) were also reactive in the presence of designed catalytic system and converted to the corresponding carbonyls in good yield and selectivity (Table 2, entries 8–10). These results confirm the high ability of Fe_3O_4@YSPMO@Ru for selective aerobic oxidation of a broad range of aliphatic and aromatic alcohols.

Next, the recoverability and reusability of Fe_3O_4@YSPMO@Ru in 1-phenylethanol oxidation were studied. To do this, after the completion of oxidation process, the catalyst was removed and it was dried and reused in conditions the same as the first run. The result showed that the Fe_3O_4@YSPMO@Ru can be recovered at least five times with no considerable decrease in performance (Fig. 9).

A hot filtration test was also performed on the above-mentioned reaction as a test model. This experiment was performed to make it clear whether the active catalytic species are leaching during the reaction process or not. To this end, after the completion of about 50% of the oxidation process, the catalyst was removed and the reaction progress of residue was monitored. Interestingly, after 10 h, no considerable conversion of alcohol was observed (Fig. 10). Moreover, the atomic absorption analysis also showed no leaching of ruthenium in the filtrate mixture. These results confirm effective immobilization and high stability of active Ru-species during the applied conditions.

Finally, the efficiency of Fe_3O_4@YSPMO@Ru was compared with some of recently reported ruthenium based heterogeneous catalysts in the oxidation of 1-phenylethanol (Table 3). As shown, the amount of applied catalyst in our study is much lower than previous studies. Moreover, the recovery times for Fe_3O_4@YSPMO@Ru is more than the former catalysts. These observations clearly confirm high catalytic efficiency and also high durability of the Fe_3O_4@YSPMO@Ru in comparison to reported catalysts.

4. Conclusion

In summary, the routine and commercially available CTAB and pluronic P123 surfactants were firstly used as efficient structure directing agents to prepare a yolk–shell nanocomposite with magnetite core and periodic mesoporous organosilica shell. This nanomaterial was effectively used for immobilization of potassium perruthenate species to deliver a novel catalyst named Fe_3O_4@YSPMO@Ru. The low angle PXRD analysis of Fe_3O_4@YSPMO@Ru confirmed the presence of a mesoporous shell for the material. The TG, FT-IR, EDX and XPS analyses showed well immobilization/incorporation and high stability of expected moieties into/onto material framework. The Fe_3O_4@YSPMO@Ru was successfully used as catalyst in the green oxidation of alcohols and gave the corresponding carbonyls in high selectivity and yield. Moreover, this catalyst was recovered and reused several times with keeping its efficiency. Therefore, this powerful and cost-effective catalyst can be promisingly used for practical applications.

Table 3 Oxidation of 1-phenylethanol using different ruthenium based heterogeneous catalysts

Entry	Catalyst	Conditions	Time (h)	Recovery times	Ref.
1	$Ru(OH)_x/Fe_3O_4$	Toluene, cat. (3.8 mol%) O_2 (1 atm), 105 °C	2	1	91
2	Fe_3O_4@SiO_2/$Ru(OH)_x$	Toluene, cat. (12.6 mol%) O_2 (10 atm), 80 °C	7	2	92
3	RuO_4@MCM-41	Toluene, cat. (1.3 mol%) O_2 (10 atm), 80 °C	24	1	93
4	Ru@PMO-IL	TFT, cat. (2.5 mol%) O_2 (1 atm), 70 °C	5.5	4	77
5	Fe_3O_4@YSPMO@Ru	TFT, cat. (0.3 mol%) O_2 (1 atm), 90 °C	6	5	This work

Conflicts of interest

There are no conflicts of interest to declare.

Acknowledgements

The authors thank the Yasouj University and the Iran National Science Foundation (INSF) for supporting this work.

References

1 Q. Wen, M. Zhang, J. Zheng and J. Xu, *CrystEngComm*, 2018, **20**, 5377–5386.
2 J. Hu, M. Zhang, L. Liu, J. Zheng, H. Alsulami, M. A. Kutbi and J. Xu, *Inorg. Chem.*, 2020, **59**, 9356–9363.
3 W. He, X. Guo, J. Zheng, J. Xu, T. Hayat, N. S. Alharbi and M. Zhang, *Inorg. Chem.*, 2019, **58**, 7255–7266.
4 X. W. D. Lou, L. A. Archer and Z. Yang, *Adv. Mater.*, 2008, **20**, 3987–4019.
5 Y. Zhao and L. Jiang, *Adv. Mater.*, 2009, **21**, 3621–3638.
6 J. Liu, S. Z. Qiao and Q. H. Hu, *Small*, 2011, **7**, 425–443.
7 J. C. Park and H. Song, *Nano Res.*, 2011, **4**, 33–49.
8 Q. Zhang, W. Wang, J. Goebl and Y. Yin, *Nano Today*, 2009, **4**, 494–507.
9 A. Cao, R. Lu and G. Veser, *Phys. Chem. Chem. Phys.*, 2010, **12**, 13499–13510.
10 J. Fan, G. Fang, X. Wang, F. Zeng, Y. Xiang and S. Wu, *Nanotechnology*, 2011, **22**, 455102.
11 C. Bharti, U. Nagaich, A. K. Pal and N. Gulati, *Int. J. Pharm. Invest.*, 2015, **5**, 124.
12 M. Zhang, L. Ding, J. Zheng, L. Liu, H. Alsulami, M. A. Kutbi and J. Xu, *Appl. Surf. Sci.*, 2020, **509**, 145348.
13 N. Lu, M. Zhang, L. Ding, J. Zheng, C. Zeng, Y. Wen, G. Liu, A. Aldalbahi, J. Shi and S. Song, *Nanoscale*, 2017, **9**, 4508–4515.
14 Y. Yin, R. M. Rioux, C. K. Erdonmez, S. Hughes, G. A. Somorjai and A. P. Alivisatos, *Science*, 2004, **304**, 711–714.
15 J. Gao, G. Liang, B. Zhang, Y. Kuang, X. Zhang and B. Xu, *J. Am. Chem. Soc.*, 2007, **129**, 1428–1433.
16 J. Liu, H. Xia, D. Xue and L. Lu, *J. Am. Chem. Soc.*, 2009, **131**, 12086–12087.
17 H. Li, Z. Bian, J. Zhu, D. Zhang, G. Li, Y. Huo, H. Li and Y. Lu, *J. Am. Chem. Soc.*, 2007, **129**, 8406–8407.
18 X.-J. Wu and D. Xu, *J. Am. Chem. Soc.*, 2009, **131**, 2774–2775.
19 G. Li, Q. Shi, S. Yuan, K. Neoh, E. Kang and X. Yang, *Chem. Mater.*, 2010, **22**, 1309–1317.
20 J. Dai, H. Zou, R. Wang, Y. Wang, Z. Shi and S. Qiu, *Green Chem.*, 2017, **19**, 1336–1344.
21 J. Liu, S. Z. Qiao, S. Budi Hartono and G. Q. Lu, *Angew. Chem., Int. Ed.*, 2010, **49**, 4981–4985.
22 J. Liu, H. Q. Yang, F. Kleitz, Z. G. Chen, T. Yang, E. Strounina, G. Q. M. Lu and S. Z. Qiao, *Adv. Funct. Mater.*, 2012, **22**, 591–599.
23 J. Liu, B. Wang, S. B. Hartono, T. Liu, P. Kantharidis, A. P. Middelberg, G. Q. M. Lu, L. He and S. Z. Qiao, *Biomaterials*, 2012, **33**, 970–978.
24 J. Liu, S. Z. Qiao, S. Budi Hartono and G. Q. M. Lu, *Angew. Chem.*, 2010, **122**, 5101–5105.
25 L. Zhang, S. Qiao, Y. Jin, Z. Chen, H. Gu and G. Q. Lu, *Adv. Mater.*, 2008, **20**, 805–809.
26 S.-H. Wu, C.-T. Tseng, Y.-S. Lin, C.-H. Lin, Y. Hung and C.-Y. Mou, *J. Mater. Chem.*, 2011, **21**, 789–794.
27 Y. E. Yan and F. W. Schwartz, *Environ. Sci. Technol.*, 2000, **34**, 2535–2541.
28 Z. Miao, X. Gu, S. Lu, X. Zang, X. Wu, M. Xu, L. B. B. Ndong, Z. Qiu, Q. Sui and G. Y. Fu, *Chemosphere*, 2015, **119**, 1120–1125.
29 R. Broséus, S. Vincent, K. Aboulfadl, A. Daneshvar, S. Sauvé, B. Barbeau and M. Prévost, *Water Res.*, 2009, **43**, 4707–4717.
30 G. Moussavi, A. Yazdanbakhsh and M. Heidarizad, *J. Hazard. Mater.*, 2009, **171**, 907–913.
31 W. Kujawski, A. Warszawski, W. Ratajczak, T. Porebski, W. Capała and I. Ostrowska, *Desalination*, 2004, **163**, 287–296.
32 W. Zhang, L. Chen, L. Xu, H. Dong, H. Hu, Y. Xiao, M. Zheng, Y. Liu and Y. Liang, *J. Colloid Interface Sci.*, 2019, **537**, 562–568.
33 C. Yao, A. Yuan, H. Zhang, B. Li, J. Liu, F. Xi and X. Dong, *J. Colloid Interface Sci.*, 2019, **533**, 144–153.
34 U. Kurt, O. Apaydin and M. T. Gonullu, *J. Hazard. Mater.*, 2007, **143**, 33–40.
35 K. Bowden, I. Heilbron, E. Jones and B. Weedon, *J. Chem. Soc.*, 1946, 39–45.
36 E. J. Corey and J. W. Suggs, *Tetrahedron Lett.*, 1975, **16**, 2647–2650.
37 G. Piancatelli, A. Scettri and M. D'auria, *Synthesis*, 1982, **1982**, 245–258.
38 A. De, *J. Sci. Ind. Res.*, 1982, **41**, 484–494.
39 F. A. Luzzio and F. S. Guziec Jr, *Org. Prep. Proced. Int.*, 1988, **20**, 533–584.
40 J. Ladbury and C. Cullis, *Chem. Rev.*, 1958, **58**, 403–438.
41 A. J. Fatiadi, *Synthesis*, 1976, **1976**, 65–104.
42 R. J. Taylor, M. Reid, J. Foot and S. A. Raw, *Acc. Chem. Res.*, 2005, **38**, 851–869.
43 K. Pfitzner and J. Moffatt, *J. Am. Chem. Soc.*, 1963, **85**, 3027–3028.
44 A. J. Mancuso, S.-L. Huang and D. Swern, *J. Org. Chem.*, 1978, **43**, 2480–2482.
45 A. J. Mancuso, D. S. Brownfain and D. Swern, *J. Org. Chem.*, 1979, **44**, 4148–4150.
46 T. T. Tidwell, *Synthesis*, 1990, **1990**, 857–870.
47 D. Dess and J. Martin, *J. Org. Chem.*, 1983, **48**, 4155–4156.
48 M. Frigerio and M. Santagostino, *Tetrahedron Lett.*, 1994, **35**, 8019–8022.
49 M. Uyanik and K. Ishihara, *Chem. Commun.*, 2009, 2086–2099.
50 J. R. Parikh and W. v. E. Doering, *J. Am. Chem. Soc.*, 1967, **89**, 5505–5507.
51 P. Lucio Anelli, C. Biffi, F. Montanari and S. Quici, *J. Org. Chem.*, 1987, **52**, 2559–2562.
52 A. E. De Nooy, A. C. Besemer and H. van Bekkum, *Synthesis*, 1996, **1996**, 1153–1176.
53 M. V. De Souza, *Mini-Rev. Org. Chem.*, 2006, **3**, 155–165.

54 T. Vogler and A. Studer, *Synthesis*, 2008, **2008**, 1979–1993.
55 R. Ciriminna and M. Pagliaro, *Org. Process Res. Dev.*, 2009, **14**, 245–251.
56 S. Patnaik, D. P. Sahoo and K. Parida, *J. Colloid Interface Sci.*, 2020, **560**, 519–535.
57 S. S. Stahl, *Angew. Chem., Int. Ed.*, 2004, **43**, 3400–3420.
58 T. Nishimura, T. Onoue, K. Ohe and S. Uemura, *J. Org. Chem.*, 1999, **64**, 6750–6755.
59 M. J. Schultz, C. C. Park and M. S. Sigman, *Chem. Commun.*, 2002, 3034–3035.
60 G. J. t. Brink, I. W. Arends, M. Hoogenraad, G. Verspui and R. A. Sheldon, *Adv. Synth. Catal.*, 2003, **345**, 1341–1352.
61 J. A. Mueller, C. P. Goller and M. S. Sigman, *J. Am. Chem. Soc.*, 2004, **126**, 9724–9734.
62 M. J. Schultz, S. S. Hamilton, D. R. Jensen and M. S. Sigman, *J. Org. Chem.*, 2005, **70**, 3343–3352.
63 M. Grßinne, *Chem. Commun.*, 2010, **46**, 7238–7240.
64 P. R. Kasturi, R. Harivignesh, Y. S. Lee and R. K. Selvan, *J. Colloid Interface Sci.*, 2020, **561**, 358–371.
65 A. Dijksman, A. Marino-González, A. Mairata i Payeras, I. W. Arends and R. A. Sheldon, *J. Am. Chem. Soc.*, 2001, **123**, 6826–6833.
66 R. Lenz and S. V. Ley, *J. Chem. Soc., Perkin Trans. 1*, 1997, 3291–3292.
67 M. Hasan, M. Musawir, P. N. Davey and I. V. Kozhevnikov, *J. Mol. Catal. A: Chem.*, 2002, **180**, 77–84.
68 A. Goti and M. Romani, *Tetrahedron Lett.*, 1994, **35**, 6567–6570.
69 A. Goti, F. De Sarlo and M. Romani, *Tetrahedron Lett.*, 1994, **35**, 6571–6574.
70 S. V. Ley, C. Ramarao and M. D. Smith, *Chem. Commun.*, 2001, 2278–2279.
71 J. Li, Z. Liu and R. Wang, *J. Colloid Interface Sci.*, 2018, **531**, 204–215.
72 K. Mori, T. Hara, T. Mizugaki, K. Ebitani and K. Kaneda, *J. Am. Chem. Soc.*, 2004, **126**, 10657–10666.
73 T. Hayashi, T. Inagaki, N. Itayama and H. Baba, *Catal. Today*, 2006, **117**, 210–213.
74 H. Wang, Z. Jusys and R. Behm, *J. Power Sources*, 2006, **154**, 351–359.
75 L. Dong, R. R. S. Gari, Z. Li, M. M. Craig and S. Hou, *Carbon*, 2010, **48**, 781–787.
76 T. Fey, H. Fischer, S. Bachmann, K. Albert and C. Bolm, *J. Org. Chem.*, 2001, **66**, 8154–8159.
77 B. Karimi, D. Elhamifar, O. Yari, M. Khorasani, H. Vali, J. H. Clark and A. J. Hunt, *Chem.–Eur. J.*, 2012, **18**, 13520–13530.
78 D. Elhamifar, O. Yari and B. Karimi, *J. Colloid Interface Sci.*, 2017, **500**, 212–219.
79 D. Elhamifar, Z. Ramazani, M. Norouzi and R. Mirbagheri, *J. Colloid Interface Sci.*, 2018, **511**, 392–401.
80 Y. S. Kang, S. Risbud, J. F. Rabolt and P. Stroeve, *Chem. Mater.*, 1996, **8**, 2209–2211.
81 S. Hajati, S. Tougaard, J. Walton and N. Fairley, *Surf. Sci.*, 2008, **602**, 3064–3070.
82 S. Hajati, V. Zaporojtchenko, F. Faupel and S. Tougaard, *Surf. Sci.*, 2007, **601**, 3261–3267.
83 V. L. Malinovskii, F. Samain and R. Häner, *Angew. Chem.*, 2007, **119**, 4548–4551.
84 A. Christopher and K. Jeremy, *J. Am. Chem. Soc.*, 1990, **112**, 5525–5534.
85 S. Balakrishnan and S. P. Sarma, *Biochemistry*, 2017, **56**, 4346–4359.
86 Q. Hou, R. Bourgeas, F. Pucci and M. Rooman, *Sci. Rep.*, 2018, **8**, 1–13.
87 N. J. Vickers, *Curr. Biol.*, 2017, **27**, R713–R715.
88 T. Chen, M. Li and J. Liu, *Cryst. Growth Des.*, 2018, **18**, 2765–2783.
89 D. P. Malenov and S. D. Zarić, *Coord. Chem. Rev.*, 2020, **419**, 213338.
90 D. P. Malenov and S. D. Zarić, *CrystEngComm*, 2019, **21**, 7204–7210.
91 Y. Zhao, J. Li, S. Zhang and X. Wang, *RSC Adv.*, 2014, **4**, 32710–32717.
92 Y. Zhao, X. Wang, J. Li and X. Wang, *Polym. Chem.*, 2015, **6**, 5376–5384.
93 X. W. Lou, L. A. Archer and Z. Yang, *Adv. Mater.*, 2008, **20**, 3987–4019.